Molecular Crystals and Liquid Crystals

Publication details, including instructions for authors and subscription information:
http://www.tandfonline.com/loi/gmcl20

C_2-Symmetric Bis(amide) Molecules: Solid-State Assembly, Thermal Stability, and Second Harmonic Generation

S. Philip Anthony† [a], M. Jaya Prakash [a] & T. P. Radhakrishnan [a]

[a] School of Chemistry, University of Hyderabad, Hyderabad, India

Version of record first published: 22 Sep 2010

To cite this article: S. Philip Anthony†, M. Jaya Prakash & T. P. Radhakrishnan (2007): C_2-Symmetric Bis(amide) Molecules: Solid-State Assembly, Thermal Stability, and Second Harmonic Generation, Molecular Crystals and Liquid Crystals, 473:1, 67-85

To link to this article: http://dx.doi.org/10.1080/15421400701432438

Mol. Cryst. Liq. Cryst., Vol. 473, pp. 67–85, 2007

ISSN: 1542-1406 print/1563-5287 online
DOI: 10.1080/15421400701432438

Taylor & Francis
Taylor & Francis Group

C_2-Symmetric Bis(amide) Molecules: Solid-State Assembly, Thermal Stability, and Second Harmonic Generation

S. Philip Anthony[†]
M. Jaya Prakash
T. P. Radhakrishnan
School of Chemistry, University of Hyderabad, Hyderabad, India

Chiral C_2-symmetric bis(amide) molecules, N,N′-bis(4-fluorobenzoyl)-(1R,2R)-diaminocyclohexane (BFBDC), N,N′-bis(4-nitrobenzoyl)-(1R,2R)-diaminocyclohexane (BNBDC), N,N′-bis(4-methoxybenzoyl)-(1R,2R)-diaminocyclohexane (BMBDC), and N,N′-bis(4-aminobenzoyl)-(1R,2R)-diaminocyclohexane (BABDC) are synthesized, and their assembly patterns in the solid state are investigated through single-crystal X-ray analysis. A range of noncovalent interactions give rise to helical superstructures in the crystals. The compounds exhibit good optical transparency and high thermal stability; these may be attributed to the specific molecular structure and extended supramolecular interactions. BMBDC and BABDC molecules possess the largest hyperpolarizabilities in the series owing to the presence of electron-donating groups and exhibit second harmonic generation (SHG) in the solid state. The optical transparency, thermal stability, and SHG capability make these materials potentially interesting candidates for quadratic nonlinear optical applications.

Keywords: bis(amide) molecule; helical superstructure; second harmonic generation

INTRODUCTION

Molecular crystals, with their fast and efficient nonlinear optical (NLO) responses, are important candidates for applications such as second harmonic generation (SHG). Wide variations that can be realized in the material attributes through the design and synthesis of

[†]Present address: National Creative Research Center for Block Copolymer Self-Assembly, Department of Chemical Engineering, Pohang University of Science and Technology, Pohang, Kyungbuk 790-784, Korea.

Address correspondence to T. P. Radhakrishnan, School of Chemistry, University of Hyderabad, Hyderabad 500 046, India. E-mail: tprsc@uohyd.ernet.in

the molecular building blocks and their assembly are key to the versatility of this class of materials. However, critical issues such as thermal and mechanical stability and optical transparency have limited the deployment of molecular materials in NLO applications. The molecular units for the construction of SHG materials should possess strong hyperpolarizability (β) and good transparency in the spectral range of interest. Noncentrosymmetric structure is an essential condition for the material to exhibit quadratic NLO effects, and optimal molecular orientations in the crystal lattice are required to elicit strong SHG responses [1,2]. Homochirality ensures the formation of a noncentrosymmetric lattice; however, the realization of optimal molecular orientations required for exhibiting efficient SHG remains a challenging problem. It is of considerable interest in this context that strong enhancement of SHG has been observed in crystals and Langmuir-Blodgett (LB) films with helical supramolecular organization [3–6]; the chirality of helical assemblies spans the whole molecular superstructure. H-bonding as well as metal coordination have been important tools for the design of extended helical assemblies. It is significant in this context that intermolecular interactions can be exploited not only in the formation of stable and structurally well-defined supramolecular structures but also enhance the thermal stability of the resulting molecular materials [7].

Chiral C_2-symmetric molecules are convenient building blocks for helical superstructures [3–5,8,9]. In an effort to improve the thermal attributes and structural organization of the C_2-symmetric diaminocyclohexane derivatives, we have incorporated amide groups as a potential H-bond functionality [10] in the molecular structure. Recently, we investigated two parent compounds in the series, N,N′-bis(benzoyl)-(1*R*,2*R*)-diaminocyclohexane (BBDC) and N,N′-bis(isonicotinoyl)-(1*R*,2*R*)-diaminocyclohexane (BINDC) [9]. It was shown that the subtle variation in the molecular structure leads to the generation of very different organizational motifs in the two crystals: polar organization promoted by the rare *syn* conformation of the bis(amide) group in BBDC and a helical organization in BINDC. The carbonyl moiety of the amide group acts as a potential electron sink, although the amino group tends to reduce the electron-withdrawing effect. Therefore, the molecular hyperpolarizability of BBDC is expected to change in a sensitive way depending on the nature of the substituents in the *para* position of the phenyl ring. In addition to exploring molecular assemblies with helical organization and high thermal stability, we investigated the impact of the *para* substituents on the hyperpolarizabilities of BBDC and hence on the SHG of the molecular crystals by synthesizing two derivatives with electron-withdrawing groups (fluoro and nitro) and two with

electron-donating groups (methoxy and amino). We have communicated earlier the salient observations in this set of compounds [9]. We now present details of the molecular structure and solid-state assembly of the chiral vicinal bis(amide) derivatives of (1*R*,2*R*)-diaminocyclohexane, N,N′-bis(4-fluorobenzoyl)-(1*R*,2*R*)-diaminocyclohexane (BFBDC), N,N′-bis(4-nitrobenzoyl)-(1*R*,2*R*)-diaminocyclohexane (BNBDC), N,N′-bis(4-methoxybenzoyl)-(1*R*,2*R*)-diaminocyclohexane (BMBDC) and N,N′-bis(4-aminobenzoyl)-(1*R*,2*R*)-diaminocyclohexane (BABDC). An extended H-bond network involving the amide groups and other substituents leads to two- and three- dimensional supramolecular structures in these crystals. Interestingly, all the crystals exhibit helical organization mediated by a range of noncovalent interactions. Nonlinear optical studies showed that molecules with electron-donating groups in the *para* position of the aromatic rings are SHG active, whereas those with electron-withdrawing groups do not show any detectable SHG; computed molecular β values provide insight into these observations. We also present electronic absorption measurements and detailed calorimetric studies that respectively demonstrate the optical transparency of the new materials and their high thermal stability.

EXPERIMENTAL

Synthesis and Characterization

1,2-Diaminocyclohexane was resolved following the methodology reported by Jacobsen *et al.* [11]. Synthesis of BFBDC, BNBDC, and BMBDC followed the general procedure reported in [12]. In each case, 2 mmol of the relevant aroyl chloride and 2.4 mmol of triethylamine were dissolved in chloroform and stirred for 10 min. One mmol of (1*R*,2*R*)-diaminocyclohexane in chloroform was added to the resulting solution. Addition was carried out slowly because of the exothermic nature of the reaction. A white precipitate formed, and the reaction mixture was heated at reflux for 14 h. The solution was then cooled to 30°C, and the solid filtered out. In some cases, the solvent was evaporated to recover the solid. The resulting off-white solid was washed with water, saturated sodium bicarbonate solution, and then again water. The product was dried under vacuum and purified by recrystallization from methanol. Single crystals were grown by slow evaporation of methanol solution.

N,N′-Bis(4-Flurobenzoyl)-(1R,2R)-Diaminocyclohexane (BFBDC)

Yield: 90%. Mp: 266°C; UV-vis (methanol solution) λ_{max} ($\lambda_{cut\text{-}off}$): 226.0 nm (279.4 nm); IR (KBr pellet): $\bar{\nu}$ (cm^{-1}): 3304.3, 2941.7,

2858.7, 1631.9, 1606.8, 1541.2, 1502.7, 1332.9, 846.8, 765.8, 665.5; ^{1}H NMR (d_6-DMSO): δ (ppm) = 1.43–1.48 (m, 4H), 1.87 (m, 2H), 2.22 (m, 2H), 4.04 (m, 2H), 6.9 (d, 4H), 6.96 (m, 2H), 7.68 (d, 4H); ^{13}C NMR (d_6-DMSO): δ (ppm) = 24.8, 32.2, 54.6, 115.2, 115.6, 129.2, 130.2, 165.2.

N,N′-Bis(4-Nitrobenzoyl)-(1R,2R)-Diaminocyclohexane (BNBDC)

Yield: 95%. Mp: 340°C (dec.); UV-vis (methanol solution) λ_{max} ($\lambda_{cut\text{-}off}$): 265.5 nm (352.0 nm); IR (KBr pellet): $\bar{\nu}$ (cm^{-1}): 3288.9, 2930.1, 2856.8, 1637.7, 1597.2, 1537.4, 1516.2, 1340.6, 869.9, 846.8, 692.5; ^{1}H NMR (d_6-DMSO): δ (ppm) = 1.28 (m, 2H), 1.57 (m, 2H), 1.78 (m, 2H), 1.91 (m, 2H), 3.99 (m, 2H), 7.93 (d, 4H), 8.26 (d, 4H), 8.68 (d, 2H); ^{13}C NMR (d_6-DMSO): δ (ppm) = 24.9, 31.6, 53.3, 123.6, 128.8, 140.8, 149.0, 164.9.

N,N′-Bis(4-Methoxybenzoyl)-(1R,2R)-Diaminocyclohexane (BMBDC)

Yield: 90%. Mp: 268°C; UV-vis (methanol solution) λ_{max} ($\lambda_{cut\text{-}off}$): 252.0 nm (289.8 nm); IR (KBr pellet): $\bar{\nu}$ (cm^{-1}): 3310.1, 2934.0, 2852.9, 1628.1, 1606.8, 1537.4, 1504.6, 1329.1, 1253.8, 1176.1, 1024.1, 839.1, 767.7, 665.5; ^{1}H NMR (d_6-DMSO): δ (ppm) = 1.28 (m, 2H), 1.50 (m, 2H), 1.72 (m, 2H), 1.93 (m, 2H), 3.76 (s, 6H), 3.88 (m, 2H), 6.92 (d, 4H), 7.40 (d, 4H), 8.10 (m, 2H); ^{13}C NMR (d_6-DMSO): δ (ppm) = 19.9, 27.4, 49.5, 50.2, 108.6, 121.7, 123.7, 157.1, 162.8.

N,N′-Bis(4-Aminobenzoyl)-(1R,2R)-Diaminocyclohexane (BABDC)

BNBDC (0.5 g, 1.2 mmol) was dissolved in dry methanol, and a catalytic amount (0.075 g) of Pd/C was added and stirred for 15 min at 30°C. $NaBH_4$ (0.5 g, 13.2 mmol) was added over 1 h. The reaction mixture was stirred further for 3 h at 30°C. Progress of the reaction was monitored by thin-layer chromatography (TLC). After completion of the reaction, Pd/C was removed by filtration. The colorless methanol solution was evaporated under reduced pressure, and water was added to the resulting product to yield a white precipitate. The precipitate was filtered and washed with sodium bicarbonate solution and water; it was then dried under vacuum. The product was purified by recrystallization from methanol. Single crystals were grown by slow evaporation of methanol solution. Yield: 0.38 g, 90%. Mp: 295°C (dec.); UV-vis (methanol solution) λ_{max} ($\lambda_{cut\text{-}off}$): 280.0 nm (327.5 nm); IR (KBr pellet): $\bar{\nu}$ (cm^{-1}): 3468.3, 3356.4, 3288.9, 2932.1, 2854.9, 1612.6, 1537.4, 1506.5, 1323.3, 1184.4, 839.1, 767.7, 574.8; ^{1}H NMR (d_6-DMSO): δ (ppm) = 1.26–1.38 (m, 4H), 1.70 (m, 2H), 1.92 (m, 2H), 3.74 (s, 2H), 5.55 (s, 4H), 6.47 (d, 4H), 7.46 (d, 4H). 7.81 (s, 2H);

^{13}C NMR (d_6-DMSO): δ (ppm) = 24.8, 32.07, 53.6, 112.7, 121.4, 128.8, 151.7, 163.6.

^{1}H and ^{13}C NMR spectra were recorded on Bruker 200-MHz or 400-MHz NMR spectrometer. Infrared spectra were collected on a Jasco 5300 FTIR spectrometer. We reported the circular dichroism spectra of these C_2-symmetric molecules earlier [9]. Electronic spectra were recorded on a Shimadzu UV 3101 PC spectrophotometer. Measurements on solid samples were made in reflectance mode using the integrating sphere attachment (ISR 3100) and converted to absorption profiles using the Kubelka-Munk function. Melting transition temperatures were measured on a TA Instruments DSC 2010 differential scanning calorimeter; scan rate of 5°C/min was employed. Other thermal studies (DTA and TGA) are presented in the supplementary information.

Crystallography

X-ray diffraction data were collected on a Bruker Nonius Smart Apex diffractometer (with CCD detector). MoK_α radiation with a graphite crystal monochromator in the incident beam was used. Data was reduced using the program SAINT; all nonhydrogen atoms were found using the direct method analysis in SHELXTL [13]. After several cycles of refinement, the positions of the hydrogen atoms were calculated and added to the refinement process. Details of data collection, solution, and refinement, as well as full crystallographic data, are submitted as supplementary information. The crystallographic data have been deposited with reference numbers CCDC 638973–638976.

SHG Measurement

Second harmonic generation from microcrystalline powders was examined using the Kurtz–Perry method [14]. Particle sizes were graded using standard sieves; sizes 30–300 μm were studied. Samples were loaded in glass capillaries having an inner diameter of 600 μm. Fundamental beam (1064 nm) of a Q-switched ns-pulsed (6 ns, 10 Hz) Nd:YAG laser (Spectra Physics Model INDI-40) was used. The second harmonic signal was collected using appropriate optics and detected using a monochromator, PMT and oscilloscope (Tektronix Model TDS 210, 60 MHz). Filters were used to bring the signals from all the samples in the same range. Urea with average particle size of ~175 μm was used as the reference.

RESULTS AND DISCUSSION

Molecular Assembly in Crystals

Single-crystal X-ray analysis revealed that the crystals of BFBDC, BNBDC, and BMBDC belong to the orthorhombic space group $P2_12_12_1$ and that BABDC belongs to the monoclinic space group $P2_1$ (Table 1). There is one molecule in the asymmetric unit in each case (Fig. 1); in the case of BABDC, there are also two water molecules of crystallization. The molecular structures in the four crystals are very similar. The bis(amide) group adopts the usual *anti* conformation in all the molecules so that the two carbonyl groups as well as the amide groups are oriented in opposite directions. This conformation facilitates the formation of complementary H-bonds leading to chain structures extending along the *a* axis in all the crystals (Fig. 2). The H-bond parameters in the different crystals are collected in Table 2. The H-bonded chains in turn are weaved into extended structures in the different crystals through a range of noncovalent interactions as described later.

In BFBDC, the H-bonded chains are connected through F...F interactions [15] ($r_{F25...F25} = 2.860$ Å; the sum of the van der Waals radii is 2.94 Å) and C–H...F interactions ($r_{C21...F26} = 3.494$ Å, $\theta_{C21\text{-}H21...F26} = 134.5^\circ$) (Fig. 3a). The latter interactions may be visualized as forming a helical motif along the *a* axis within the 2_1 chains (Fig. 3b). In BNBDC, the nitro groups mediate the noncovalent interactions ($r_{C14...O30} = 3.338$ Å, $\theta_{C14\text{-}H14...O30} = 128.5^\circ$; $r_{C18...O27} = 3.581$ Å, $\theta_{C18\text{-}H18...O27} = 152.3^\circ$) leading to extended assembly (Fig. 4a). One of the interactions between the aromatic CH group *meta* to the nitro group and the nitro group of a neighboring molecule leads to the helical structure propagating along the *a* axis (Fig. 4b). A number of noncovalent interactions are observed in BMBDC (Fig. 5a). In one case, methoxy groups of adjacent molecules interact with each other ($r_{C28...O25} = 3.397$ Å, $\theta_{C28\text{-}H28B...O25} = 157.8^\circ$), and in the other cases, methoxy groups interact with the carbonyl oxygen atom ($r_{C26...O10} = 3.621$ Å, $\theta_{C26\text{-}H26A...O10} = 148.9^\circ$; $r_{C28...O12} = 3.515$ Å, $\theta_{C28\text{-}H28C...O12} = 148.5^\circ$). The latter interactions possess a helical structure in the 2_1 chain extending along the *a* axis (Fig. 5b). The water molecules in the lattice of BABDC mediate several strong H-bond interactions, leading to extended noncovalent assembly (Fig. 6a). These H-bonds involve both the amide ($r_{O27...O10} = 2.871$ Å, $\theta_{O27\text{-}H27A...O10} = 171.6^\circ$; $r_{O28...O12} = 2.821$ Å, $\theta_{O28\text{-}H28A...O12} = 165.0^\circ$) and amine groups ($r_{N25...O28} = 3.098$ Å, $\theta_{N25\text{-}H25A...O28} = 163.9^\circ$; $r_{N26...O27} = 3.193$ Å, $\theta_{N26\text{-}H26B...O27} = 157.3^\circ$). The helical structure formed through these

TABLE 1 Crystallographic Data for BFBDC, BNBDC, BMBDC, and BABDC

Compound	BFBDC	BNBDC	BMBDC	BABDC · $2H_2O$
Empirical formula	$C_{20}H_{20}F_2N_2O_2$	$C_{20}H_{20}N_4O_6$	$C_{22}H_{26}N_2O_4$	$C_{20}H_{28}N_4O_4$
Formula weight	358.38	412.40	382.45	388.46
Crystal system	Orthorhombic	Orthorhombic	Orthorhombic	Monoclinic
Space group	$P2_12_12_1$ (No. 19)	$P2_12_12_1$ (No. 19)	$P2_12_12_1$ (No. 19)	$P2_1$ (No. 4)
a (Å)	5.0889(3)	5.0133(9)	5.0789(5)	5.1297(4)
b (Å)	18.8303(11)	17.922(3)	19.1500(18)	21.2093(17)
c (Å)	18.8509(11)	22.016(4)	20.9714(19)	9.4739(8)
β (°)	90	90	90.0	99.158(2)
V $(Å)^3$	1806.40(18)	1978.1(6)	2039.7(3)	1017.60(14)
Z	4	4	4	2
ρ_{calc} (g cm^{-3})	1.318	1.385	1.245	1.268
μ $(mm^{-1)}$	0.100	0.104	0.086	0.090
λ (Å)	0.71073	0.71073	0.71073	0.71073
2θ range (°)	1.53–28.26	1.47–28.23	1.44–28.27	1.92–28.31
Unique reflections	4321	4728	4778	4722
Reflection with $I \geq 2\sigma_I$	1809	1956	2388	3164
Number of parameters	235	270	255	269
GOF	0.800	0.832	0.859	0.882
R [for $I \geq 2\sigma_I$]	0.0425	0.0494	0.0443	0.0494
wR^2 [for $I \geq 2\sigma_I$]	0.0589	0.0594	0.0680	0.0786
Largest difference peak, hole ($eÅ^{-3}$)	0.096, −0.118	0.173, −0.145	0.114, −0.117	0.200, −0.150

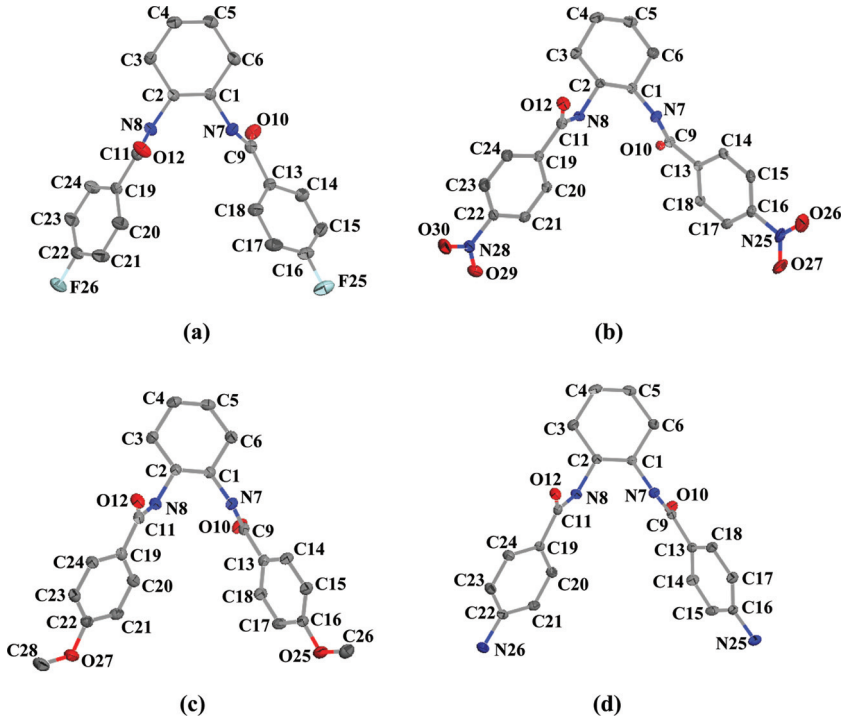

FIGURE 1 Molecular structure of (a) BFBDC, (b) BNBDC, (c) BMBDC, and (d) BABDC from single-crystal x-ray structure analysis. H atoms are omitted for clarity; C (grey), N (blue), O (red), and F (cyan) atoms with 65% probability thermal ellipsoids are indicated.

H-bond interactions is shown in Fig. 6b. The various intermolecular short contacts described illustrate the extended interactions that lead to possible cooperative binding of the molecules in the different crystals.

Second Harmonic Generation

Even though the carbonyl group in the amide functionality is not an efficient electron acceptor, it can still act as a potential electron sink. Therefore, depending on the nature of the substituents in the *para* position of the phenyl rings in the bis(amide) molecules, their push–pull character and hence molecular hyperpolarizability can be tuned to some extent. We have estimated the β values using AM1/TDHF [16] computations implemented in the MOPAC93 program package [17].

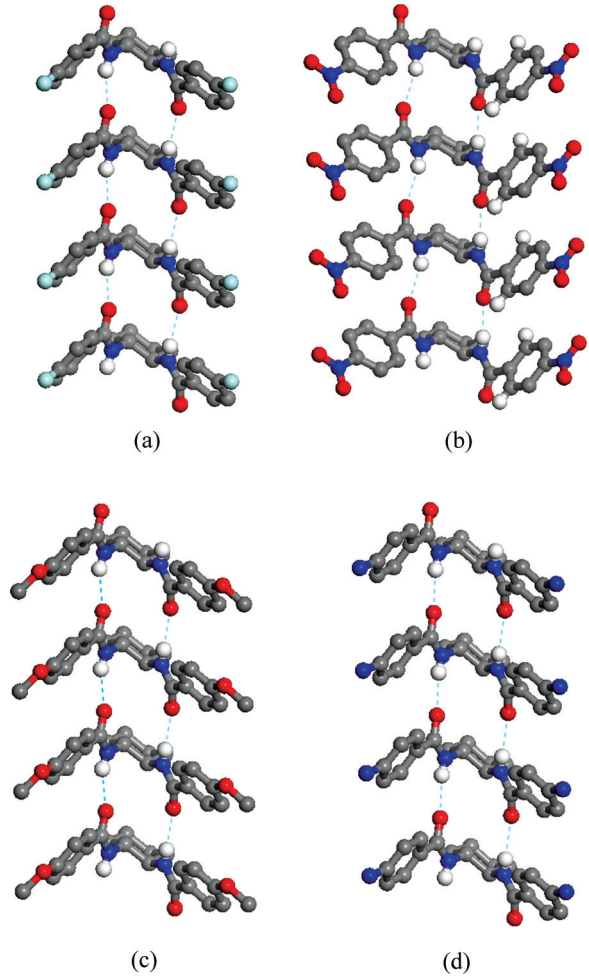

FIGURE 2 Extended structures formed along the *a* axis through complementary H-bonds involving amide groups in (a) BFBDC, (b) BNBDC, (c) BMBDC, and (d) BABDC. All H atoms except those involved in the H-bonds are omitted for clarity; C (grey), N (blue), O (red), and F (cyan) atoms and H-bonds (cyan broken lines) are indicated.

Calculations were carried out on the optimized structures of the four molecules; both static β and the value corresponding to excitation at 1064 nm were computed (Table 3). Presence of the electron-withdrawing groups, fluoro and nitro in the *para* position, leads to low β values in BFBDC and BNBDC. However, the donor groups, methoxy and

TABLE 2 Structural Parameters for the Intermolecular H-bonds Linking the Amide Groups in BFBDC, BNBDC, BMBDC and BABDC

Crystal	$r_{N7\ldots O10}$ (Å)	$\theta_{N7\text{-}H7\ldots O10}$ (°)	$r_{N8\ldots O12}$ (Å)	$\theta_{N8\text{-}H8\ldots O12}$ (°)
BFBDC	3.017	163.5	2.932	158.1
BNBDC	2.854	160.1	2.974	150.4
BMBDC	2.934	157.0	2.953	158.3
BABDC	2.976	162.2	2.977	153.0

Note. r and θ are the relevant distance and angle (atom labeling are shown in Fig. 1).

amino, effect a considerable increase in the β value of BMBDC and BABDC. These results also indirectly suggest that the carbonyl group retains its electron-withdrawing nature even though the amino nitrogen in the amide moiety tends to reduce its strength.

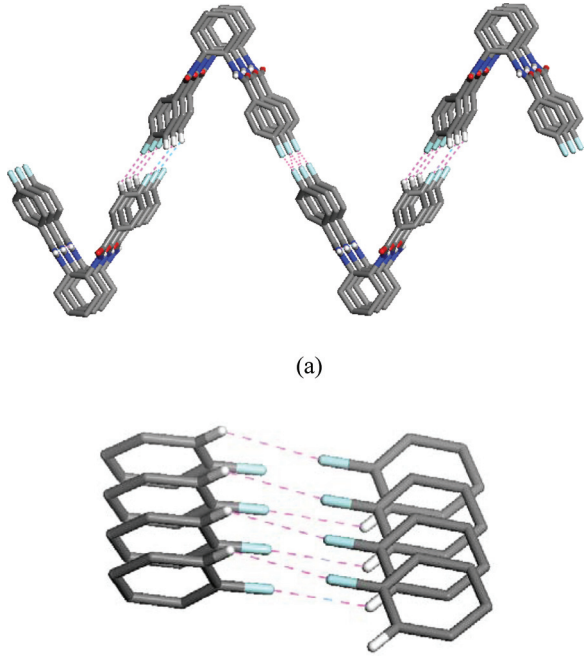

FIGURE 3 (a) Extended noncovalent interactions in BFBDC crystal (see text for details); (b) view of the structural units involved in the M helical motif.

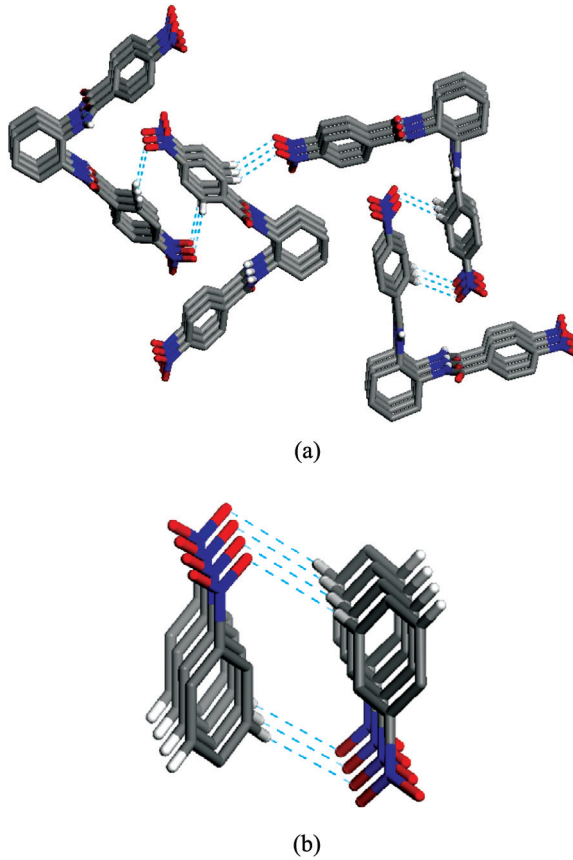

FIGURE 4 (a) Extended noncovalent interactions in BNBDC crystal (see text for details); (b) view of the structural units involved in the M helical motif.

Kurtz–Perry experiments on microcrystalline powder samples using a 1064-nm fundamental beam revealed that BFBDC and BNBDC produce no measurable SHG but that BMBDC and BABDC are active. Particle-size dependence of the SHG response (Fig. 7) indicates phase-matchable behavior in both the cases. The SHG at saturation is approximately equivalent to that of urea in the case of BMBDC and about double of that in BABDC (Table 3). Because the general crystal assembly motifs are similar in all the four crystals, the SHG of the bulk materials reflects the trends in molecular nonlinearity. The observed impact of the electron-rich groups connected to the amide functionality in improving the solid-state SHG, and

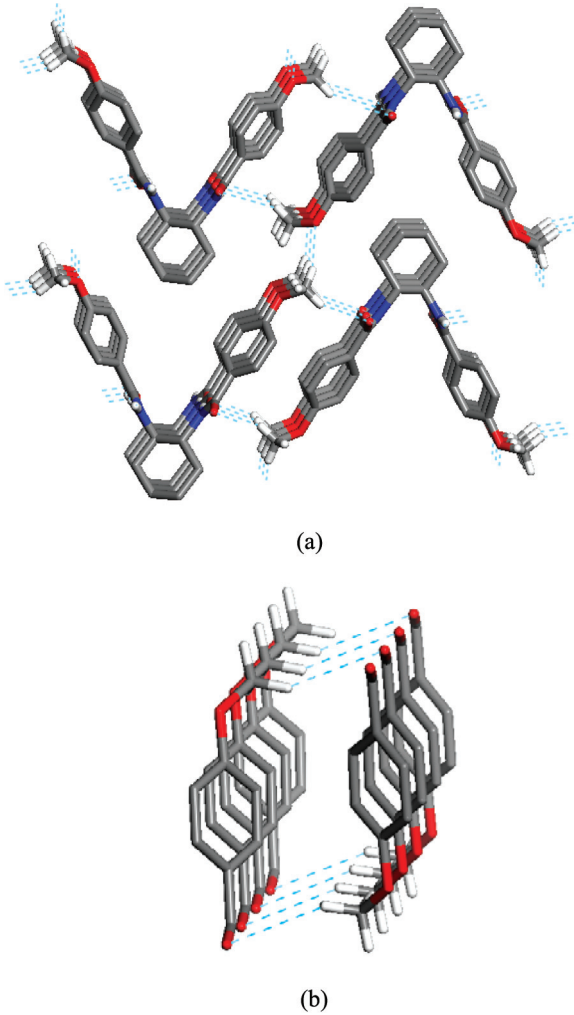

FIGURE 5 (a) Extended noncovalent interactions in BMBDC crystal (see text for details); (b) view of the structural units involved in the P helical motif.

that of the electron-poor groups in reducing it, is consistent with the classical push–pull concepts [1]. In our earlier study [4], we reported that N,N′-bis(4-cyanophenyl)-(1*R*,2*R*)-diaminocyclohexane (BCDC) exhibits an SHG of $\sim$0.3 U. It is interesting to note that BMBDC which crystallizes in the same space group as BCDC and possesses a smaller molecular hyperpolarizability, shows an SHG response three

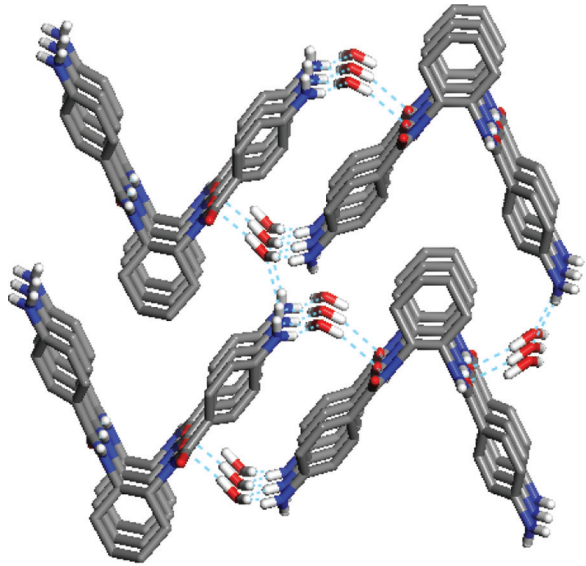

(a)

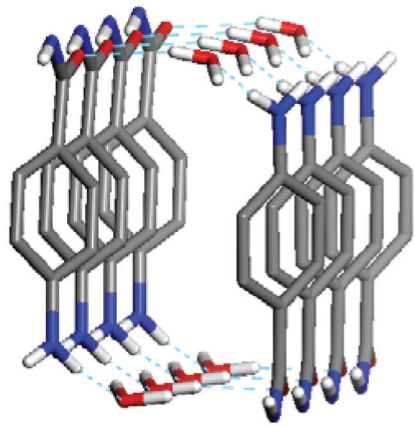

(b)

FIGURE 6 (a) Extended noncovalent interactions in BABDC crystal (see text for details); (b) view of the structural units involved in the P helical motif.

TABLE 3 AM1/TDHF Computed Hyperpolarizabilities, β (static and at 1.17 eV) of BFBDC, BNBDC, BMBDC and BABDC and the Solid-State SHG at Saturation

	β (10^{-30}esu)		
Compound	0 eV	1.17 eV	Average value of SHG/U
BFBDC	1.44	2.11	*a*
BNBDC	1.81	2.83	*a*
BMBDC	4.02	6.37	0.90
BABDC	6.47	11.29	1.82

[a]No detectable SHG.
Note. 1 U = SHG of urea with average particle size of 175 μm.

times higher. The enhanced SHG of BMBDC and BABDC is possibly facilitated by the helical supramolecular organization; BCDC molecules do not form helical assemblies, but metal coordination polymers of BCDC possess a helical structure and exhibit enhanced SHG response. We examined the stability of the four bis(amide) compounds under laser irradiation; no visible damage was observed up to $\sim$1 GW/cm^2 of laser fluence in all cases.

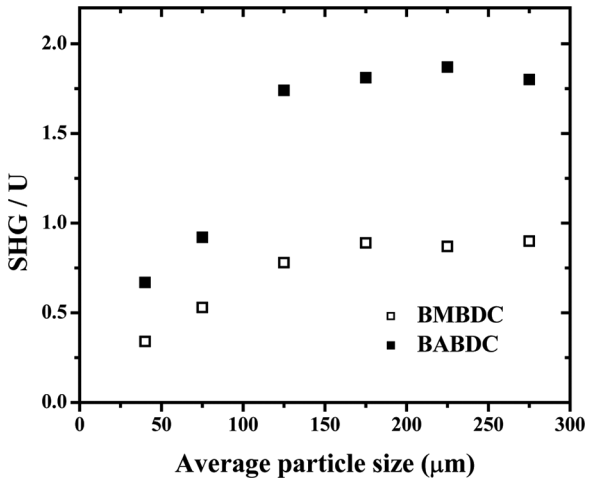

FIGURE 7 SHG from microcrystalline powders of BMBDC and BABDC with different particle sizes (1 U = SHG of urea with average particle size of 175 μm).

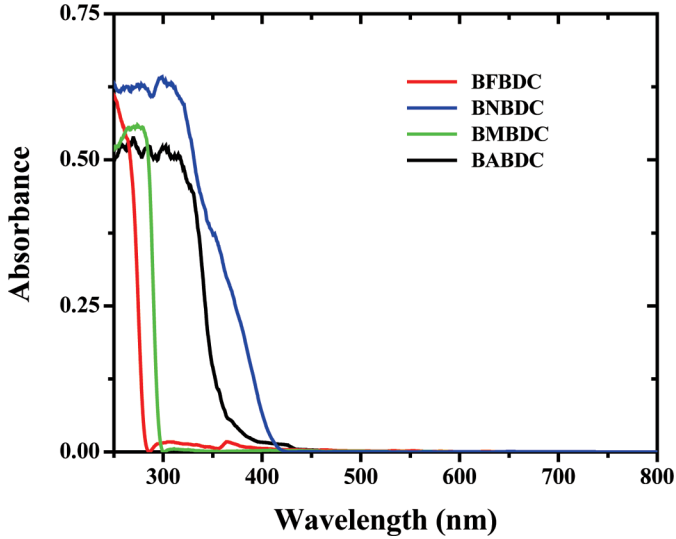

FIGURE 8 Electronic absorption spectra of BFBDC, BNBDC, BMBDC, and BABDC in the solid state.

Optical and Thermal Properties

Optical transparency and thermal stability are important attributes for SHG materials, from the point of view of application. High transmission through the visible range would preclude absorption of the second harmonic and potential materials damage arising as its consequence. The chiral bis(amide) compounds are promising materials in this regard as demonstrated by their good optical transparency in the solid state. Figure 8 shows the absorption spectra of the four compounds in the solid state; the wavelength cutoffs for their optical

TABLE 4 Wavelength Cut-Off for the Electronic Absorption in the Solid State (Based on the Extrapolation of the Absorption Edge) and Melting Point of BFBDC, BNBDC, BMBDC, and BABDC Determined from the DSC Traces

Compound	$\lambda_{cut\text{-}off}$ (nm)	Melting Point (°C)
BFBDC	282.0	266.0
BNBDC	415.5	340.0
BMBDC	297.0	267.5
BABDC	397.0	294.5

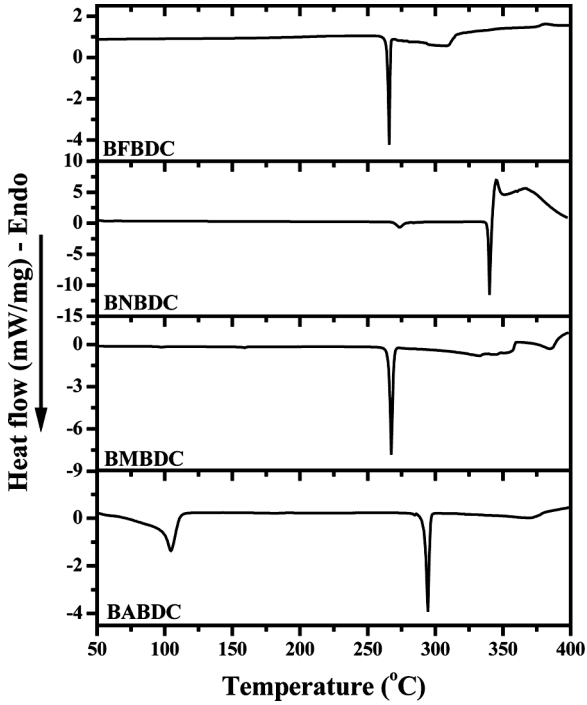

FIGURE 9 Differential scanning calorimetry traces for BFBDC, BNBDC, BMBDC, and BABDC.

absorption are listed in Table 4. Solution spectra are provided in the supplementary information. All the compounds have negligible absorption in the visible range; this possibly contributes to the stability of the materials under strong laser irradiation.

Thermal stability of these novel materials was investigated by different calorimetric methods (see also supplementary information). DSC traces of the four solids are collected in Figure 9. The high thermal-damage thresholds of the compounds are clearly demonstrated by these data; considering the fact that these are simple organic molecules, the melting temperatures (Table 4) are quite high. BABDC shows an additional transition with a peak at 104.5°C, which arises because of the loss of the water of crystallization as shown by thermogravimetric analysis. In view of their homochirality and potential to form interesting supramolecular structures, earlier we investigated several chiral C_2-symmetric diaminocyclohexane derivatives for second-order NLO applications. *N*,*N*′-Bis(4-nitrophenyl)-(1*R*,2*R*)-diaminocyclohexane (BNDC) [3] and BCDC [4] are two examples.

These compounds with nitrophenyl and cyanophenyl groups attached directly to the amine group of diaminocyclohexane melt at 204°C and 150°C, respectively. Significantly, introduction of amide functionality in the molecular structure, even without any functional groups on the phenyl group in the case of BBDC, led to an enhancement in the melting temperature to 268°C [9]; this can be attributed to the extended complementary hydrogen-bonding interactions between the amide groups. Replacing the phenyl group by pyridyl group in BINDC as well as introduction of fluoro (BFBDC) or methoxy (BMBDC) group in the *para* position of the phenyl groups of BBDC does not lead to any significant enhancement in the thermal stability. This is not surprising, because the additional intermolecular interactions in these crystals are quite weak compared to those of the amide groups already present in BBDC. However, introduction of nitro and amino groups in the *para* position of the phenyl ring in BNBDC and BABDC led to further enhancement in the melting point to 340°C and 295°C respectively, possibly through the involvement of the strong noncovalent interactions mediated by these functional groups. Thus the bis(amide) molecules with appropriate functionalization appear to provide a logical route to the establishment of thermally stable and optically transparent NLO active materials.

CONCLUSIONS

Molecular assembly in the crystals of a series of chiral C_2-symmetric bis(amide) molecules was investigated. A range of noncovalent intermolecular interactions including complementary hydrogen bonds bind the molecules into extended supramolecular assemblies with helical motifs present in all the structures. The extensive intermolecular interactions appear to be responsible for the high thermal stability of this family of compounds. All the solids show high transparency through the visible range. The molecular hyperpolarizability is sensitive to the substituents in the *para* position of the phenyl ring of the bis(amide) molecules, and this has direct bearing on the solid-state SHG response; the amino derivative has the highest SHG capability in the series. Further molecular modifications can be conceived in terms of extending the push–pull structures and enhancing the molecular hyperpolarizability so that stronger SHG responses can be realized. The thermal stability coupled with high transparency and appreciable SHG capability should make this class of compounds important candidates to develop novel quadratic nonlinear optical materials.

SUPPLEMENTARY INFORMATION AVAILABLE

Crystallographic, spectroscopic, and thermal data (24 pages) is available upon request.

ACKNOWLEDGMENTS

Financial support from the DST and CSIR, New Delhi, and the use of the National Single-Crystal Diffractometer Facility Department of Science and Technology (DST) at the School of Chemistry, University of Hyderabad, are gratefully acknowledged. S. P. A. and M. J. P. thank the Council of Scientific and Industrial Research (CSIR), New Delhi, for senior research fellowships.

REFERENCES

[1] (a) Chemla, D. S. & Zyss, J. (Eds.). (1989). *Nonlinear Optical Properties of Organic Molecules and Crystals*, Chemla, D. S. & Zyss, J. (Eds.), Academic Press: New York, Vols. 1, 2; (b) Prasad, P. N. & Williams, D. J. (1991). *Introduction to Nonlinear Optical Effects in Molecules and Polymers*, John Wiley: New York; (c) Zyss, J. & Nicoud, J. F. (1996). *Curr. Opin. Solid State Mater. Sci*., *1*, 533; (d) Günter, P. (2000). *Nonlinear Optical Effects and Materials*, Springer Series in Optical Sciences, Springer-Verlag: Heidelberg, Vol. 72.

[2] Hoss, R., König, O., Kramer-Hoss, V., Berger, U., Rogin, P., & Hulliger, J. (1996). *Angew. Chem., Int. Ed*., *35*, 1664; (b) Holman, K. T., Pivovar, A. M., & Ward, M. (2001). *Science*, *294*, 1907; (c) Anthony, S. P. & Radhakrishnan, T. P. (2001). *Chem. Commun*., *931*; (d) Anthony, S. P., Raghavaiah, P., & Radhakrishnan, T. P. (2003). *Cryst. Growth Des*., *3*, 631.

[3] Gangopadhyay, P. & Radhakrishnan, T. P. (2001). *Angew. Chem. Int. Ed*., *40*, 2451.

[4] Anthony, S. P. & Radhakrishnan, T. P. (2004). *Chem. Commun*., 1058.

[5] Xie, Y. R., Xiong, R. G., Xue, X., Chen, X. T., Xue, Z., & You, X. Z. (2002). *Inorg. Chem*., *41*, 3323; (b) Han, L., Hong, M., Wang, R., Luo, J., Lin, Z., & Yuan, D. (2003). *Chem. Commun*., 2580.

[6] Verbiest, T., Elshocht, S. V., Kauranen, M., Hellemans, L., Snauwaert, J., Nuckolls, C., Katz, T. J., & Persoons, A. (1998). *Science*, *282*, 913; (b) Kauranen, M., Verbiest, T., Elshocht, S. V., & Persoons, A. (1998). *Opt. Mater*., *9*, 286.

[7] Timofeeva, T. V., Kuhn, G. H., Nesterov, V. V., Nesterov, V. N., Frazier, D. O., Penn, B. G., & Antipin, M. Y. (2003). *Cryst. Growth Des*., *3*, 383; (b) Nesterov, V. V., Antipin, M. Y., Nesterov, V. N., Penn, B. G., Frazier, D. O., Timofeeva, T. V. (2004). *Cryst. Growth Des*., *4*, 521; (c) Nesterov, V. V., Antipin, M. Y., Nesterov, V. N., Moore, C. E., Cardelino, B. H., Timofeeva, T. V. (2004). *J. Phy. Chem. B*, *108*, 8531.

[8] Anthony, S. P. & Radhakrishnan, T. P. (2004). *Cryst. Growth Des*., *4*, 1223.

[9] Anthony, S. P., Basavaiah, K., & Radhakrishnan, T. P. (2005). *Cryst. Growth Des*., *5*, 1663.

[10] Fan, A., Valiyaveettil, S., & Vittal, J. J. (2003). *Cryst. Eng. Comm*., *5*, 38; (b) Feng, Z., Fan, A., Valiyaveettil, S., & Vittal, J. J. (2003). *Cryst. Growth. Des*., *3*, 555.

[11] Larrow, J. F., Jacobson, E. N., Gao, Y., Hong, Y., Nie, X., & Zepp, C. M. (1994). *J. Org. Chem*., *59*, 1939.
[12] Whitener, G. D., Hagadorn, J. R., & Arnold, J. (1999). *J. Chem. Soc. Dalton Trans*., *1249*.
[13] *SAINT-Plus, version 6.45*. Bruker AXS: Madison, WI (2003); (b) *SHELXTL, version 6.14*. Bruker AXS: Madison, WI (2003).
[14] Kurtz, S. K. & Perry, T. T. (1968). *J. Appl. Phys*., *39*, 3798; (b) Jayanty, S., Gangopadhyay, P., & Radhakrishnan, T. P. (2002). *J. Mater. Chem*., *12*, 2792.
[15] Reichenbächer, K., Süss, H. I., & Hulliger, J. (2005). *Chem. Soc. Rev*., *34*, 22.
[16] Dewar, M. J. S., Zoebisch, E. G., Healy, E. F., Stewart, J. J. P. (1985). *J. Am. Chem. Soc*., *107*, 3902; (b) Dupuis, M. & Karna, S. (1991). *J. Comput. Chem*., *12*, 487.
[17] *MOPAC93*, (1993). Fujitsu Inc.: Tokyo.